

Pseudo Spin Valves Using a (112)-textured $D0_{22}$ $Mn_{2.3-2.4}Ga$ Fixed Layer

C. L. Zha,¹ R. K. Dumas,¹ J. Persson,¹ S. M. Mohseni,¹ J. Nogués,^{1,3} and Johan Åkerman^{1,2}
¹*Material Physics Division, Royal Institute of Technology (KTH), Electrum 229, 164 40 Stockholm, Sweden*

²*Department of Physics, University of Gothenburg, 412 96 Gothenburg, Sweden and*

³*Institució Catalana de Recerca i Estudis Avançats (ICREA) and
Centre d'Investigació en Nanociència i Nanotecnologia (ICN-CSIC),
Campus Universitat Autònoma de Barcelona, 08193 Bellaterra, Spain*

(Dated: September 12, 2018)

Abstract- We demonstrate pseudo spin valves with a (112)-textured $D0_{22}$ $Mn_{2.3-2.4}Ga$ (MnGa) tilted magnetization fixed layer and an in-plane CoFe free layer. Single $D0_{22}$ MnGa films exhibit a small magnetoresistance (MR) typically observed in metals. In MnGa/Cu/CoFe spin valves a transition from a negative (-0.08%) to positive (3.88%) MR is realized by introducing a thin spin polarizing CoFe insertion layer at the MnGa/Cu interface and tailoring the MnGa thickness. Finally, the exchange coupling between the MnGa and CoFe insertion layer is studied using a first-order reversal curve (FORC) technique.

Index Terms- Magneto-electronics, Spin valves, $D0_{22}$ MnGa, Tilted polarizer, Negative magnetoresistance, First-order reversal curve (FORC)

I. INTRODUCTION

Since the prediction by J. Slonczewski and L. Berger that a spin polarized current can exert enough torque on a magnetic layer to significantly affect its magnetization [Slonczewski 1996, Berger 1996], the Spin-Transfer Torque effect (STT) has been intensely investigated for potential applications in spintronic devices, such as Spin-Transfer Torque Magnetoresistance Random Access Memory (STT-MRAM) [Zhu 2008], Spin Torque Oscillators (STO) [Katine 2008], and domain-wall memory [Parkin 2008]. While such devices are typically divided into in-plane and perpendicular free or fixed layer geometries, we recently proposed a so-called Tilted Polarizer STO where the fixed layer magnetization is tilted out of the film plane in order to simultaneously achieve zero field operation and high output power [Zhou 2008, Zhou 2009a]. The tilt angle introduces an additional degree of freedom, which leads to a surprisingly rich phase diagram of spin torque switching and precession [Zhou 2009b].

A tilted spin polarizer, with both in-plane and out-of-plane spin polarization components, can be experimentally achieved using materials with strong tilted magnetocrystalline anisotropy. We have previously reported on using (111)-oriented $L1_0$ FePt and FePtCu with tilted magnetocrystalline anisotropy to fabricate pseudo spin valves (PSV's) for spin torque devices [Zha 2009a, Zha 2009b, Zha 2009c]. However, $L1_0$ FePt and FePtCu have a number of drawbacks such as a relatively low spin polarization [Seki 2008], undesirably high damping factor [Seki 2006], and prohibitive cost due to its high Pt content. Very recently, $D0_{22}$ ordered $Mn_{3-x}Ga$ ($x=0\sim 1$) was theoretically predicted to be a nearly half-metallic ferrimagnet with 88% spin polarization at the Fermi surface, and was consequently proposed to have great potential for STT devices [Balke 2007, Winterlik 2008, Wu 2009]. The large magneto-crystalline anisotropy ($K_{eff}=1.2 \times 10^7$ erg/cm³), the low magnetization ($\leq M_s=250$ emu/cm³) and the expected high degree of spin polarization make

$Mn_{3-x}Ga$ ideal as a tilted polarizer [Winterlik 2008, Wu 2009], provided the appropriate crystalline orientation of the $D0_{22}$ phase can be realized.

In this Letter, we report on the successful fabrication of (112)-textured $D0_{22}$ $Mn_{2.3-2.4}Ga$ (MnGa hereafter) thin films with a tilted magnetization and pseudo spin valves based on these films. In single $D0_{22}$ MnGa films we observe a small magnetoresistance (MR) with a parabolic field dependence consistent with ordinary MR typically observed in all metals. In MnGa/Cu/CoFe PSV's a small negative giant magnetoresistance (GMR) is observed between the MnGa and CoFe layers. In order to obtain a sizable positive GMR effect an ultra-thin CoFe layer is inserted at the MnGa/Cu interface.

II. EXPERIMENTS

All film stacks were deposited at room temperature on thermally oxidized Si substrates using a magnetron sputtering system (AJA ATC Orion-8) with a base pressure better than 5×10^{-8} Torr. Deposition of a 6 nm Ta underlayer was followed by MnGa deposition from a $Mn_{60}Ga_{40}$ alloy target. This bilayer was subsequently annealed *in-situ* at 400°C for 35 min to form the $D0_{22}$ (112)-textured MnGa phase. For the PSV's a 5 nm Cu spacer and a 5 nm $Co_{50}Fe_{50}$ (CoFe) layer were deposited after cool-down to room temperature. Finally, a 3 nm Ta capping layer was deposited on both single MnGa films and PSV's for oxidation protection. Three different MnGa thicknesses of 15, 25 and 50 nm were employed to fabricate PVS's. The final $Mn_{70}Ga_{30}$ film composition was determined using energy dispersive x-ray spectrometry (EDX). Note that the achieved composition is located in the 66 to 74 at.% Mn range where the $D0_{22}$ phase is expected to appear [Niida 1996].

Magnetic properties were characterized using a Physical Property Measurement System (PPMS) equipped with a Vibrating Sample Magnetometer (VSM) and an

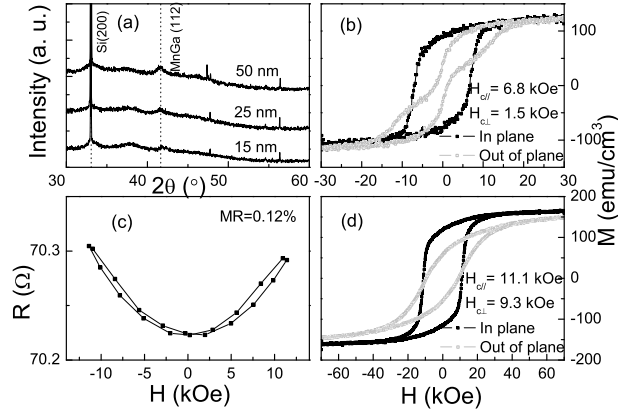


FIG. 1: (a) XRD patterns of 15 nm, 25 nm, 50 nm single MnGa films, respectively; (b) in-plane and out-of-plane VSM hysteresis loops and (c) current-in-plane magnetoresistance curve of a single 15 nm MnGa film; (d) in-plane and out-of-plane VSM hysteresis loops of a single 50 nm MnGa film.

Alternating-Gradient Magnetometer (AGM) with a maximum field of 14 kOe. In addition to standard major hysteresis loop analysis we employed a first-order reversal curve (FORC) technique [Davies 2004, Dumas 2007]. First, a family of FORC curves was measured. Each curve started at a successively more negative reversal field, H_R , and was then measured with an increasing applied field, H , parallel to the film plane. Then, a mixed second-order derivative of the magnetization, $M(H, H_R)$, was used to generate a FORC distribution, $\rho \equiv -\partial^2 M(H, H_R) / 2\partial H \partial H_R$, which was plotted against (H, H_R) coordinates on a contour map. Crystallographic structures were investigated by x-ray diffraction (XRD) with Cu K_α radiation in a symmetric scan geometry. Current-in-plane (CIP) electron transport properties were determined by a standard 4-point tester with the current orthogonal to the magnetic field (transverse configuration).

III. RESULTS AND DISCUSSION

Fig. 1 shows structural and magnetic properties of single MnGa films. Following Ref. [Winterlik 2008], we identify the peaks at 41.36° in Fig. 1(a) as the (112) diffraction peak of the $D0_{22}$ phase of $Mn_{3-x}Ga$. Importantly, with increasing film thickness we observe enhanced (112) texture as the relative diffraction intensity becomes stronger. Hysteresis loops of the 15 nm MnGa film in Fig. 1(b) exhibit in-plane coercivity ($H_{c||}$) of 6.8 kOe and out-of-plane one ($H_{c\perp}$) of 1.5 kOe, as well as a 120 emu/cm^3 saturation magnetization (M_S). A 50 nm MnGa (Fig. 1(d)) reveals $H_{c||}=11.1 \text{ kOe}$, $H_{c\perp}=9.3 \text{ kOe}$, and $M_S=160 \text{ emu/cm}^3$. These values are consistent with the ferrimagnetic structure of $D0_{22}$ MnGa film previously

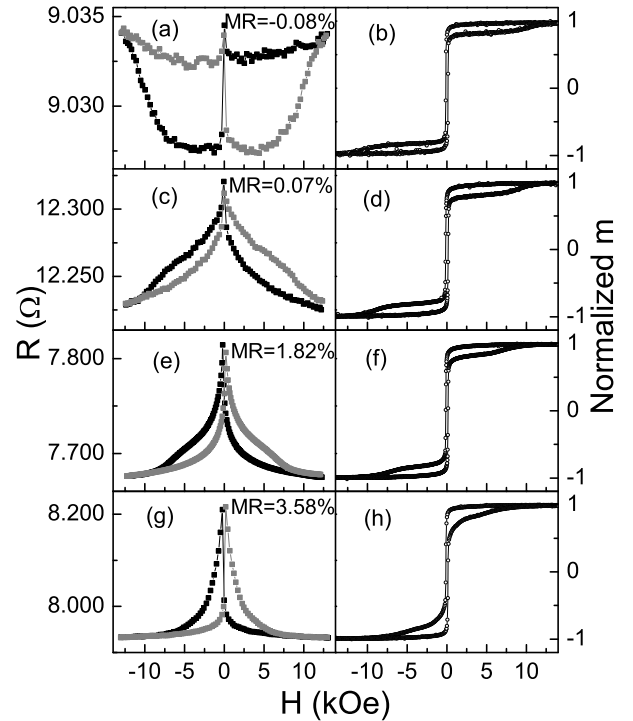


FIG. 2: Current-in-plane magnetoresistance curves (left column) and hysteresis loops (right column) of Ta (6 nm)/MnGa (15 nm)/CoFe (y nm)/Cu (5 nm)/CoFe (5 nm)/Ta (3 nm), (a, b) $y=0$; (c, d) $y=0.5$; (e, f) $y=1.0$ and (g, h) $y=1.5$.

reported [Wu 2009]. The squareness ratios of the out-of-plane and the in-plane loops are less than 1, indicating that the easy magnetization axis lies in neither the film plane nor along the normal direction, as expected for highly textured (112) $D0_{22}$ MnGa films. The improved magnetic properties of the 50 nm MnGa film are consistent with its enhanced structural properties, Fig. 1(a). This indicates that the chemical ordering of the $D0_{22}$ phase of MnGa increases (inducing a higher magnetocrystalline anisotropy) with thickness under the same annealing condition. The CIP-MR is found to be 0.12% at ± 14 kOe for the 15 nm single MnGa film, Fig. 1(c), which we ascribe to ordinary magnetoresistance of a metal. A relatively large residual resistance of about 70 Ohm implies a moderate crystallinity, consistent with the XRD results (Fig. 1(a)).

The magnetotransport and magnetic properties of PSV's of MnGa (15 nm)/CoFe(0, 0.5, 1.0, 1.5 nm)/Cu (5 nm)/CoFe(5 nm) are shown in Fig. 2. The unique shape of the MR curve in Fig. 2(a), for MnGa/Cu/CoFe, is due to a combination of effects. The most prominent contribution to the MR is a negative GMR between the CoFe and MnGa layers. Near positive saturation the two layers are parallel and a relatively high resistance state is observed. As the applied field is reduced (dark filled squares) a

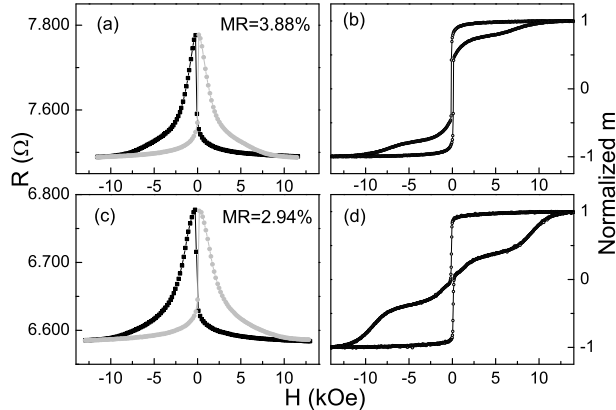


FIG. 3: CIP-MR curves (a, c) and in-plane AGM hysteresis loops (b, d) of Ta (6 nm)/MnGa (25 nm)/CoFe (1.5 nm)/Cu (5 nm)/CoFe (5 nm)/Ta (3 nm) and Ta (6 nm)/MnGa (50 nm)/CoFe (1.5 nm)/Cu (5 nm)/CoFe (5 nm)/Ta (3 nm), respectively.

sharp drop in resistance near zero field is observed as the CoFe (5 nm) free layer switches and becomes anti-parallel to the MnGa layer. With a further decrease in applied field the resistance remains nearly constant until roughly -5kOe where the MnGa layer begins to switch. Finally, a high resistance state, corresponding to parallel alignment of the CoFe and MnGa, is once again achieved at negative saturation. This situation is similar to Fe/Cu/GdCo spin valves [Yang 2006] and FeCoGd/AlO/FeCo tunnel junctions [Bai 2008] where a negative GMR is also observed. In addition to the dominant negative GMR contribution a small peak in the resistance near zero field is also observed and is most likely due to either anisotropic MR in the transverse measurement geometry or a small positive GMR component. Finally, a small parabolic background, most obvious at high fields, is observed due to the ordinary MR of the MnGa layer, similar to Fig. 1(c).

CoFe usually gives positive bulk and interface spin asymmetry coefficients with Cu [Li 2002]. Considering, *ab initio* calculations [Winterlik 2008] of the electronic structure for $D0_{22}$ Mn_3Ga , it is found that the minority (majority) density of states exhibits a maximum (minimum) at the Fermi energy and the bulk spin asymmetry coefficient is positive [Tsymbal 1996]. However, based on the negative GMR found in this PSV, Fig. 2(a), we could not rule out the possibility of a negative interface spin asymmetry coefficient at the MnGa/Cu interface. To obtain a positive interface spin asymmetry coefficient we employ a thin CoFe insertion layer at the MnGa/Cu interface. We therefore expect to not only obtain conventional positive GMR, as anticipated for a PSV, but also enhancement of the MR [Vouille 1999].

As shown in Fig. 2(c), when an ultrathin 0.5 nm CoFe layer is inserted between the spacer and fixed layers,

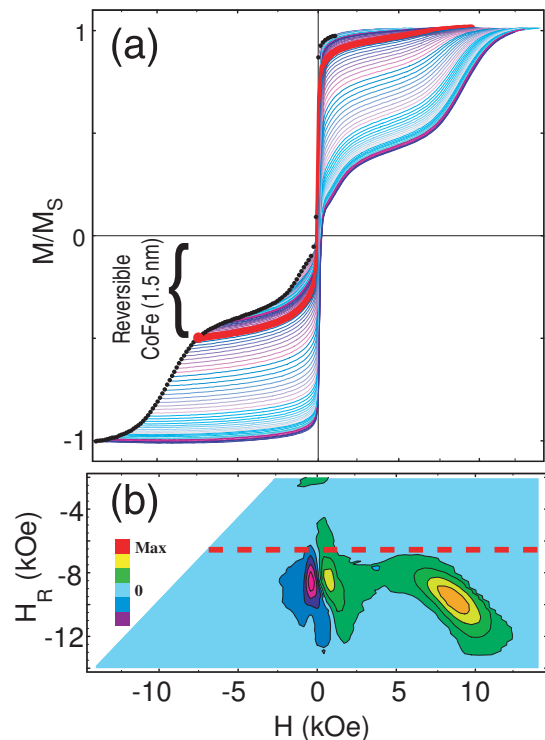


FIG. 4: (Color online) (a) A family of FORC curves and (b) the FORC diagram of MnGa (50 nm)/CoFe (1.5 nm)/Cu (5 nm)/CoFe (5 nm) spin valve. The red horizontal dashed line indicates the onset of irreversible switching.

we find a positive MR of 0.07%. This suggests that GMR from spin-dependent interface scattering at the CoFe/Cu/CoFe interfaces is greater than net negative MR from MnGa alone. The MR is found to increase further as the thickness of the CoFe insertion layer is increased as shown in Figs. 2(e) and (g). The shape of the MR loops indicates a two-step switching for spin valves, which progressively weakens as the CoFe insertion layer becomes thicker, virtually disappearing for 1.5 nm layers. On the other hand, the easy magnetization axis is probably gradually pushed into the film plane by the thicker CoFe.

The hysteresis loops in Figs. 2(b, d, f, h) show a two-stage switching which leads to the observed GMR effect. The large vertical separation between the upper and lower plateaus in the hysteresis loops is due to the much higher moment (4 times as high) of the CoFe free layer than the fixed layer. With increasing thickness of the CoFe insertion layer the switching plateau becomes gradually smaller and the coercivity of the MnGa fixed layer also gradually decreases, indicating the switching of the soft CoFe insertion layer assists the hard MnGa switching due to exchange interactions.

To further improve current-in-plane magnetoresistance, we explore the effect of the MnGa thickness on magnetotransport. As shown in Figs. 3(a) and (c), MR increases to 3.88% when $t_{MnGa} = 25$ nm. However, when in-

creasing the thickness of MnGa to 50 nm we find the MR decreases to 2.95%. This decrease is most likely due to current shunting through the relatively thick MnGa layer [Zha 2009d]. Figs. 3(b) and (d) exhibit the in-plane magnetic properties for these two spin valves with $t_{MnGa}=25$ and 50 nm. The separate switching between the free CoFe layer and the fixed MnGa/CoFe bilayer corresponds to GMR.

To better understand the interaction between the CoFe insertion layer and MnGa fixed layer the FORC technique is employed. The family of measured FORC curves is shown in Fig. 4(a) where black dots represent the starting point for each FORC. As the reversal field is decreased a sharp drop in magnetization is found near $H_R \sim 0$ kOe which corresponds to the CoFe free layer switching. This is a highly irreversible process and manifests itself as a very narrow peak with a large intensity for reversal fields $H_R \sim 0$ Oe in the FORC distribution. To highlight the switching of the MnGa (50 nm)/CoFe (1.5 nm) bilayer alone the FORC distribution is plotted for $H_R < -2$ kOe in Fig. 4(b). Interestingly, the FORC diagram is nearly featureless for $-6.5 \text{ kOe} < H_R < -2 \text{ kOe}$ indicating reversible switching processes. This region is also highlighted with a bracket in Fig. 4(a) and is associated with the highly reversible switching of the CoFe insertion layer. The onset of irreversible switching occurs for reversal fields $H_R < -6.5$ kOe which is indicated with a horizontal dashed line in Fig. 4(b) and the red bold FORC in Fig. 4(a). For $H_R < -6.5$ kOe we begin to see peaks in the FORC distribution that corresponds to irreversible switching of the MnGa layer as negative saturation is approached. We can interpret the reversal of the MnGa (50 nm)/CoFe (1.5 nm) bilayer as being that of a classic bilayer exchange-spring magnet [Davies 2005, Fullerton 1998, Nagahama 1998] where the MnGa and CoFe can be identified as the hard and soft components, respectively. This exchange spring interaction explains the lack of a two-step behavior in the MR data in samples with thick CoFe insertion layers. Essentially, after the CoFe free layer switches, the CoFe insertion layer begins to reversibly switch leading to a gradual decrease in the MR as saturation is approached.

IV. CONCLUSION

In summary, PSV's using (112)-textured D0₂₂ MnGa as a fixed layer have been demonstrated and a MR up to 3.88% has been achieved. A negative GMR is observed in MnGa/Cu/CoFe spin valves. However, a negative to positive transition in the MR is realized by insertion of a thin CoFe layer at the MnGa/Cu interface. Reversal of the MnGa/CoFe bilayer has been analyzed and shows exchange-spring like behavior which explains the lack of a two-step reversal typically observed in the MR response of spin valves. These results are encouraging for future spintronic devices such as STO's where MnGa will be an advantageous spin polarizer.

ACKNOWLEDGMENT

We are grateful to S. Lidin for giving us access to the PPMS. C.Z. thanks Dr. Ngoc Anh Nguyen Thi for fruitful discussions. Support from The Swedish Foundation for strategic Research (SSF), The Swedish Research Council (VR), the Göran Gustafsson Foundation, and the Knut and Alice Wallenberg Foundation is gratefully acknowledged. J.N. thanks the Wenner Gren Center Foundation, the Catalan DGR (2009SGR1292) and the Spanish MICINN (MAT2007-66309-C02) projects for partial financial support. J.Å. is a Royal Swedish Academy of Sciences Research Fellow supported by a grant from the Knut and Alice Wallenberg Foundation.

REFERENCES

- Bai XJ, Du J, Zhang J, You B, Sun L, Zhang W, et al (2008), *J. Appl. Phys.*, vol. 103, pp. 07F305.
- Balke B, Fecher GH, Winterlik J, and Felser C (2007), *Appl. Phys. Lett.*, vol. 90, pp. 152504.
- Berger L (1996), *Phys. Rev. B*, vol. 54, pp. 9353-9358.
- Davies JE, Hellwig O, Fullerton EE, Denbeaux G, Kostright JB, and Liu K (2004), *Phys. Rev. B*, vol. 70, pp. 224434.
- Davies JE, Hellwig O, Fullerton EE, Jiang JS, Bader SD, Zimanyi GT, and Liu K (2005), *Appl. Phys. Lett.*, vol. 86, pp. 262503
- Dumas RK, Li CP, Roshchin IV, Schuller IK, and Liu K (2007), *Phys. Rev. B*, vol. 75, pp. 134405
- Fullerton EE, Jiang JS, Grimsditch M, Sowers CH, and Bader SD (1998), *Phys. Rev. B*, vol. 58, pp. 12193
- Katine JA and Fullerton EE (2008), *J. Magn. Magn. Mater.*, vol. 320, pp. 1217-1226.
- Li M, Liao S, and Ju K (2002), US Patent 6683762.
- Nagahama T, Mibu K, and Shinjo T (1998), *J. Phys D: Appl. Phys.*, vol. 31, pp. 43
- Niida H, Hori T, Onodera H, Yamaguchi Y, and Nakagawa Y (1996), *J. Appl. Phys.*, vol. 79, pp. 5946-5948.
- Parkin SSP, Hayashi M, and Thomas L (2008), *Science*, vol. 320, pp. 190-194.
- Seki T, Hasegawa Y, Mitani S, Takahashi S, Imamura H, Maekawa S, et al (2008), *Nat. Mater.*, vol. 7, pp. 125-129.
- Seki T, Mitani S, Yakushiji K, and Takanashi K (2006), *Appl. Phys. Lett.*, vol. 88, pp. 172504.
- Slonczewski JC (1996), *J Magn. Magn. Mater.*, vol. 159, pp. L1-L7.
- Tsymbal EY, and Pettifor DG (1996), *Phys. Rev. B*, vol. 54, pp. 15314-15329 .
- Vouille C, Barthélémy A, Mpondo FE, Fert A, Schroeder PA, Hsu SY, et al (1999), *Phys. Rev. B*, vol. 60, pp. 6710-6722.
- Winterlik J, Balke B, Fecher GH, Alves MCM, Bernardi F, and Morais J (2008), *Phys. Rev. B*, vol. 77, pp. 054406.

Wu F, Mizukami S, Watanabe D, Naganuma H, Oogane M, Ando Y, et al (2009), *Appl. Phys. Lett.*, vol. 94, pp. 122503.

Yang DZ, You B, Zhang XX, Gao TR, and Zhou SM, Du J (2006), *Phys. Rev. B*, vol. 74, pp. 024411.

^aZha CL, Persson J, Bonetti S, Fang YY, and Åkerman J (2009), *Appl. Phys. Lett.*, vol. 94, pp. 163108.

^bZha CL, Bonetti S, Persson J, Zhou Y, and Åkerman J (2009), *J. Appl. Phys.*, vol. 105, pp. 07E910.

^cZha CL, Fang YY, Nogués J, and Åkerman J (2009),

J. Appl. Phys., vol. 106, pp. 053909.

^dZha CL, and Åkerman J (2009), *IEEE Trans. Mag.*, vol. 45, pp. 3491-3494.

Zhou Y, Zha CL, Bonetti S, Persson J, and Åkerman J (2008), *Appl. Phys. Lett.*, vol. 92, pp. 262508.

^aZhou Y, Zha CL, Bonetti S, Persson J, and Åkerman J (2009), *J. Appl. Phys.*, vol. 105, pp. 07D116.

^bZhou Y, Bonetti S, Zha CL, and Åkerman J (2009), *New J. of Phys.*, vol. 11, pp. 103028.

Zhu JG (2008), *Proc. IEEE*, vol. 96, pp. 1786-1798.